Advanced Detection of Rotor Electrical Faults in Induction Motors at Start-up

Advanced Detection of Rotor Electrical Faults in Induction Motors at Start-up

Konstantinos N. Gyftakis, *Senior Member, IEEE,* Dionysios V. Spyropoulos, *Member, IEEE* and Epaminondas D. Mitronikas, *Member, IEEE*

***Abstract*—It has been lately shown that, traditional diagnostic approaches for rotor electrical faults detection in induction motors can be dangerously misleading. That is due to many different fault cases that mask the fault signatures thus leading to false negative alarms, or a plethora of harmless conditions that generate signatures similar to the faulty ones leading to false positive alarms. Aiming for reliable fault detection, a new trend has appeared, that of the analysis of the stator current at start-up of the motor. This method proves to be reliable in many cases, however there are still cases where it can lead to false positive alarms especially when applied on motors by diagnostic engineers for the first time. Aiming for a more reliable approach, a new method is proposed in this paper. The proposed novel method consists of the analysis of the zero-sequence current under transient motor operation and specifically the start-up. The paper's findings demonstrate the method's reliability and superiority over the analysis of a single current.**

***Index Terms*—Condition monitoring, Fault diagnosis, Induction motor, Transient analysis, Zero-sequence current**

I. Introduction

INDUCTION machines are among the most widespread power devices in the world due to their robustness, low cost, easy control and good efficiency. They consist the most well spread motoring devices in industry in a number of applications such as pumps, mills, conveyors and elevating machines [1]. They have also been used as traction motors in electric vehicle applications [2]. As generators, they can be mostly found in wind energy harvesting [3] and small hydro plants [4]. Lately, they have appeared in marine applications such as wave and tidal energy generation [5].

Since induction machines are dominating in the power world, they are related to the power and industrial production countries worldwide and therefore the economy. Their uninterrupted and safe operation is crucial to guarantee significant incomes. Despite that, a variety of stresses act on the machines and lead to degradation and ageing. Such stresses are known as the TEAM (Thermal, Electrical, Ambient and Mechanical) [6]. Progressive degradation over time will lead to early faults which in most cases are not immediately catastrophic. If however, such incipient fault stages are left undetected, they evolve in severity and will lead to a catastrophic machine breakdown [7]. The impact of a breakdown is severe as it typically leads to huge financial losses for the inspection and repair of the machine as well as the losses due to the lack of production. Also, delays in the delivery of products are expected because faulty machines require significant time periods before reoperation [8]. Furthermore, in remote applications or machines in harsh environments, conventional diagnostic approaches cannot be applied. It becomes evident that the need for reliable, remote and on-line condition monitoring is of the outmost importance.

The paper is dealing with rotor electrical faults detection in induction motors. Such faults have become popular lately because the classical and established approaches such as the MCSA (Motor Current Signature Analysis) are no longer deemed reliable to detect them. Magnetic anisotropy [9], axial cooling rotor air-ducts [10]-[12], porosity [13]-[14], fan blades number [15] and load oscillations [16] can all lead to false positive diagnostic alarms when the MCSA is applied. Furthermore, the fault signatures are masked under several cases such as; non-adjacent broken bars [17]-[19], broken bars at the upper cage of double cage motors [20]-[21] and operation under low or no load [22]-[23]. Since those signatures depend on the slip, an erroneous speed estimation may also lead to misdiagnosis.

Aiming to improve the diagnostic reliability, a modern trend has emerged. According to this philosophy, it is better to monitor the stator current during the start-up and analyze it in time-frequency domain. Works utilizing the Short Time Fourier Transform (STFT) [24],[25], the Adaptive Slope Transform (AST) [25] the Wavelets [25]-[29],the MUSIC algorithms [30] and the Wigner-Ville Distribution (WVD) [25],[31]for the analysis of the stator current and the stray flux have shown very promising results. However, the sensitivity of the current's transient analysis method is in some cases low because it is influenced by the motor's inherent electromagnetic rotor asymmetries as it will be shown later in this work.

Aiming for an improved resolution towards a reliable fault diagnosis method, this paper proposes the use of the zero-sequence current (ZSC) harmonic index during the motor's starting as an improved alternative to the existing technical

K. N. Gyftakis is with the School of Engineering and the Institute for Energy Systems, The University of Edinburgh, The King's Buildings, Edinburgh, EH93FB, UK (e-mail: k.n.gyftakis@ieee.org).

D. V. Spyropoulos and E. D. Mitronikas are with the Dept. of Electrical and Computer Engineering, University of Patras, Rion, Patras, 26500, Greece. (e-mail: dionspyrop@ece.upatras.gr, e.mitronikas@ece.upatras.gr).

know-how. It will be shown via finite element simulations and experimental testing that the ZSC spectrograms via the STFT are quite immune to inherent rotor asymmetries while the fault related signatures present far higher amplitudes than those of a single current, thus the chances of a misdiagnosis are eliminated. The method is applicable in motors connected in delta or star with the neutral accessible.

II. Theoretical Investigation

It is well known that, when a bar breaks from the rotor cage a counter rotating magnetic field (opposite with respect to the main rotating magnetic field) is generated in the rotor. This new field has frequency sf_s. Due to the mechanical speed this component induces voltage back to the stator at frequency $(1-2s)f_s$. The speed ripple effect will create a right-hand sideband in the stator current at $(1+2s)f_s$.

However, the stator current has a rich harmonic index due to the saturation, which will be expressed in terms of odd multiples of the supply frequency: $(2k \pm 1)f_s, k \in \mathbb{N}$. Following a similar reasoning, the broken bar fault causes harmonics at frequencies [23]:

$$f_{bb} = \left[\frac{k}{p}(1-s) \pm s\right] f_s, k \in \mathbb{N} \quad (1)$$

When a healthy induction motor is connected in delta, the phase currents contain all odd multiples of the supply frequency. The triplets or in other words the harmonics that are odd multiples of three and the fundamental frequency are in phase between the three phases (e.g. 3rd, 9th etc.). Consequently, they cancel out from the line currents, which contain harmonics at $(6k \pm 1)f_s, k \in \mathbb{N}$ (e.g. 1st, 5th, 7th, 11th etc.). In star connected machines (without the neutral connected), the phase currents and the line currents are the same and the triplets do not exist.

The ZSC is equal to one third of the instantaneous sum of the three phase currents:

$$i_{ZSC} = \frac{1}{3}(i_a + i_b + i_c) \quad (2)$$

Therefore, in star connected machines (without the neutral connected), the ZSC is zero. On the other hand, in delta connected machines the ZSC is equal to the sum of the triplets and circulates in the delta loop. Therefore, its fundamental harmonic is the 3rd, which is also known to be saturation dependent [24]. The same goes for star connected machines with the neutral connected. The ZSC will flow through the neutral back to the source.

Since the 3rd harmonic is the fundamental harmonic of the ZSC, the primary expected broken rotor bar signatures are expected at frequencies: $(3-2s)f_s$ and $(3-4s)f_s$ according to equation (1). Those are the main fault indicators, however a theoretical trajectories map is shown in Fig. 1, to include the PSH and 9th harmonic as well, although the latter might not be that strong especially in larger machines.

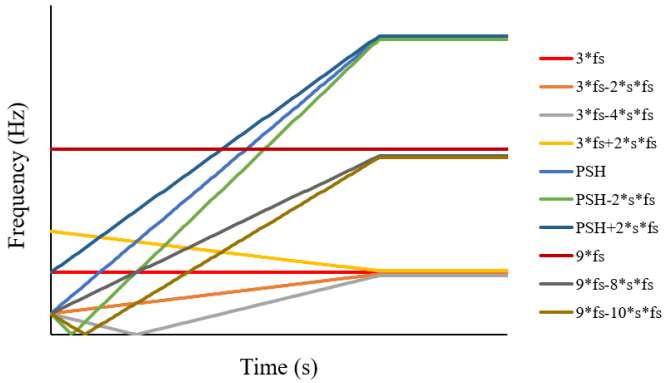

Fig. 1. Broken bar fault trajectories in the zero-sequence current spectrogram.

Based on the above theoretical investigation, a series of advantages of the ZSC over a single current analysis can be demonstrated as follows.

A. Improved Diagnosis at Low Slip Operation

One of the main drawbacks in detecting broken bars is the slip dependency of the produced signatures. It has been reported that for very low slip, the fault signatures, which are distanced by $\pm 2sf_s$ from the fundamental harmonic, may fall in the spectral leakage of the fundamental and their information is hidden.

In the case of the ZSC, the same will happen to the $(3-2s)f_s$, however the second signature at $(3-4s)f_s$ has double frequency distance and may yet be observable.

B. Saturation Impact

At low load operation, the saturation level of the machine's iron core is maximized due to the maximization of the voltage across the magnetizing inductance. The fundamental ZSC harmonic is saturation dependent, which means that its amplitude and consequently the associated fault signatures' amplitudes will be enhanced by an increased saturation level.

C. Skin and Proximity Effects Impact

When a conductor carries AC current, the current density tends to be higher towards the surface of the conductor and on the inside, it decreases exponentially. This current displacement leads to an increase of the conductor's resistance. This phenomenon is known as the skin effect. Moreover, when two neighboring conductors carry AC currents they will induce currents to each other due to Faraday's law of induction, which will distort the current density distribution. The impact of both phenomena increases with the frequency.

Therefore, since the ZSC fundamental has 3 times greater frequency than that of a single current, the skin and proximity effects will appear stronger leading to an enhancement of the magnetic asymmetry caused by the broken bar, thus leading to higher amplitudes of the associated harmonics (normalized with respect to each individual fundamental). Furthermore, stronger amplitudes of the harmonics are also expected, due to derivation of the flux due to Faraday's law of induction in order to generate the induced stator voltage the amplitude of which depends on the frequency.

D. Spectral Resolution under Fast Transient Operation

The starting of a motor depends on several parameters, which determine the shaft acceleration from stall to steady state. Such parameters are the output motor torque, the load torque and the combined moment of inertia of the motor's rotor and that of the mechanical load. Since this time varies between different machines and applications, it affects the captured number of periods of the recorded signal. The ZSC has three times greater frequency than the fundamental stator current one, which leads to the conclusion that, it offers an improved spectral resolution for fast transients because under any fixed amount of time, three times more ZSC periods will be captured than a single stator current.

III. Finite Element Analysis

This section deals with the analysis of different power sized induction motors under healthy and faulty conditions with the use of the Finite Element Analysis (FEA). The goal is to study the detectability of the broken bar fault via the single stator and the ZSC currents at startup. FEA is a great methodology because it allows for very reliable results, taking into account all non-linear electromagnetic phenomena while the operating conditions are ideal. The results are therefore free from the influence of inherent manufacturing motor asymmetries as well as source imbalances and instrumentation tolerances, conditions always present in experimental testing.

Two different sized motors are used, the rated characteristics of which are shown in Table I. Due to their significantly different moment of inertia, the two motors have a different starting time from stall to steady state, which is more approximately double in the large motor compared to the smaller one. Both motors have been simulated under healthy operation and under broken rotor bar faults.

TABLE I
Rated Characteristics of the Two Simulated Motors

Characteristics	Motor A	Motor B
Connection	Y	Δ
Nominal Voltage	6.6 kV	400 V
Frequency	50Hz	50Hz
Rated Power	1.1 MW	4 kW
Number of poles	6	4
Stator slots	54	36
Rotor slots	70	32

To be more specific, Motor A has been simulated under one and two adjacent broken bars, while Motor B only with 1 broken bar. The reason behind this choice lies in the need for a fair severity comparison due to the different number of bars and magnetic poles between the two motors. Motor A has 11.67 rotor bars per magnetic pole while Motor B has 8 bars per magnetic pole. So, if one bar breaks in both machines, the fault impact and therefore the magnetic field asymmetry is expected to be greater in Motor B. This is why Motor A has been simulated under 2 broken bars also, to bring the magnetic asymmetry between the two motors closer and allow for a fair comparison. The two simulated motors and their cross-sectional magnetic flux density distribution are shown in Fig. 2 below. The field asymmetry due to the broken bar is shown with an arrow.

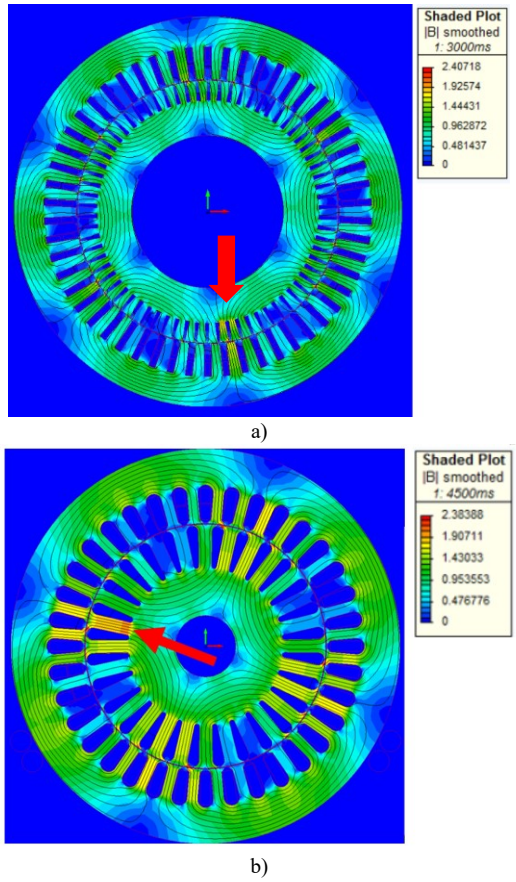

Fig. 2. Cross-sectional flux distribution of: a) Motor A and b) Motor B under rated operation at steady state.

Firstly, a single stator current of Motor A is analyzed with the STFT for healthy operation and under 1 and 2 broken bars (adjacent). A Blackman window was used with length 4096 points and overlap 1/8 of the window's length. The number of FFT points was also 4096.

The spectrograms are presented in the following Fig. 3. Due to the long starting time, the spectrogram under faulty conditions offers a very clear overview of the generated fault harmonics' trajectories. The strongest fault trajectory is obviously the $(1-2s)f_s$ which creates the well-known V shape below the fundamental 50 Hz harmonic (black arrow). Other trajectories such as the $(1+2s)f_s$ (purple arrow) and the $(5-4s)f_s$ (red arrow) are also clear in both faulty cases. Finally, the $(1\pm4s)f_s$ (yellow arrows) and the $(5-2s)f_s$ (orange arrow) harmonics are clear in the motor with 2 broken bars.

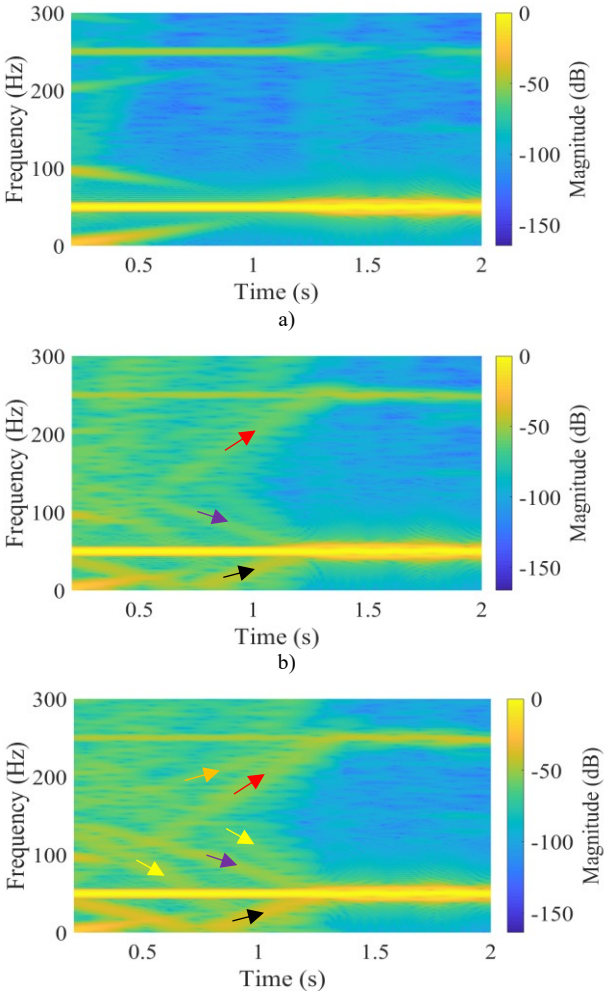

Fig. 3. STFT spectrogram of a single stator current of Motor A under: a) healthy operation, b) 1 broken bar and c) 2 broken bars.

Secondly, the line current of Motor B is analyzed with the STFT for healthy operation and under 1 broken bar (Fig. 4). It is to be noted that the starting time is approximately half than that of Motor A. This leads lower resolution and the trajectories of the fault harmonics are not very clear especially their part below 0.3 s. The main harmonics that can be identified however with low clarity are the $(1-2s)f_s$ (black arrow) and the $(5-4s)f_s$ (red arrow).

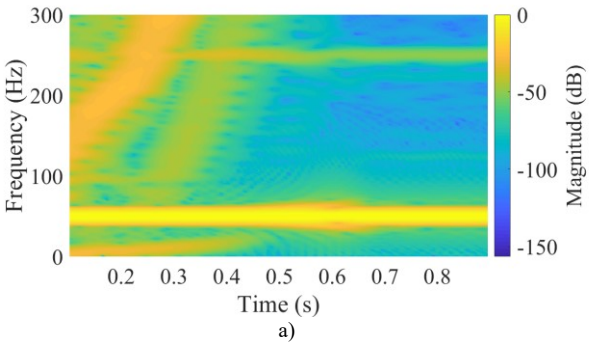

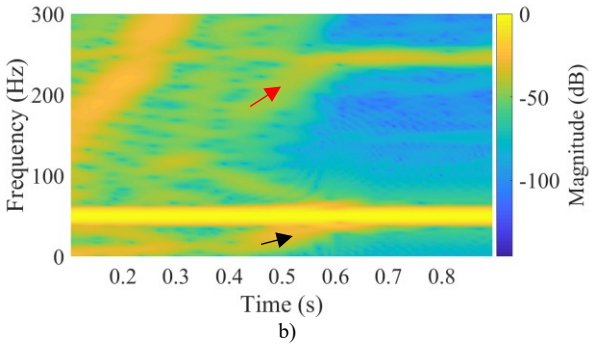

Fig. 4. STFT spectrogram of a single stator line current of Motor B under: a) healthy operation and b) 1 broken bar.

Considering that Motor B is connected in delta, the phase current carries some additional harmonics compared to the line current as explained in Section II. The triplets do not exist in the line current under symmetrical operation and this is clear in Fig. 3-b. Despite that, the phase current includes the triplets and associated fault signatures. The spectrogram of the phase current is presented in Fig. 5 below. The trajectories of the fault signatures at $(3-2s)f_s$ (red arrow) and $(3-4s)f_s$ (black arrow) are quite clear, especially the former one. The trajectory of the latter is clear only above the 50 Hz harmonic's trajectory.

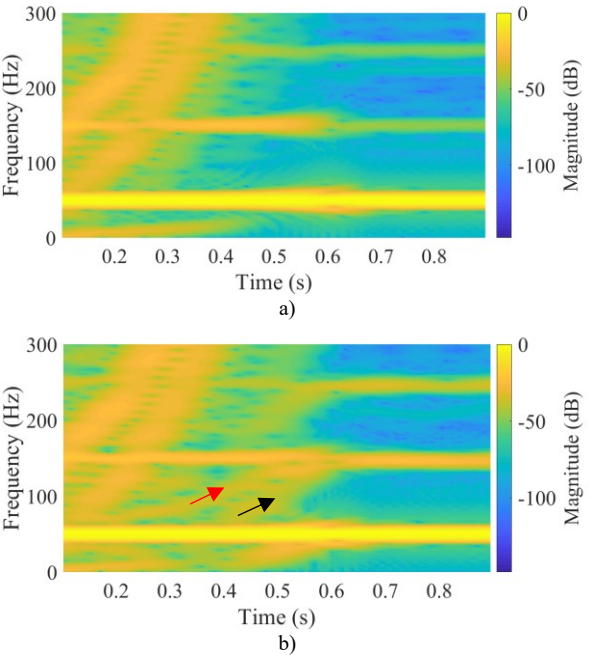

Fig. 5. STFT spectrogram of a single stator phase current of Motor B under: a) healthy operation and b) 1 broken bar.

A comparison of the spectral resolution between the signatures of the fundamental and the third harmonic reveals that the faulty trajectories associated with the third one are significantly clearer. The reasons behind the improved clarity around the third harmonic have already been explained in detail in Section II. A use of a high pass filter could isolate the third harmonic, however its associated fault signatures with V shape expand until the 0 Hz (e.g. $(3-4s)f_s$ which becomes 0 Hz for slip s=0.75). The best way to filter out the fundamental

harmonic completely without any distortion of the third harmonic and associated fault sidebands is through the calculation of the ZSC, that is the instantaneous sum of the three phase current waveforms. Then all harmonics with phase difference 120 degrees such as the $(6k \pm 1)f_s$ will cancel out leaving only the triplets in the ZSC.

Following the above methodology, the ZSC has been calculated in Motor B and its spectrogram is shown in Fig. 6 for healthy and faulty operating conditions.

There are two harmonics in the ZSC with important amplitudes in the healthy motor case. The fundamental current harmonic at 50 Hz as well as the fifth at 250 Hz are non-existent. The third fundamental ZSC harmonic and one more, which has variable frequency over time, can be observed. This harmonic is the low Principle Slot Harmonic (PSH) with frequency: $\left[\frac{N_R}{p}(1-s)-1\right]f_s$. The studied motor has 32 rotor slots and 4 poles, which means that the rotor slots number is an integer multiple of the number of poles. Consequently, the motor produces the PSH. The low PSH is in phase between the phase currents thus it passes on to the ZSC. This however is not of interest for this paper, which focuses on the detectability of the broken rotor bars. The two main sidebands of the third harmonic appear very clearly and with great amplitudes in the case of the fault as shown in Fig. 6-b. The two signatures are the $(3-2s)f_s$ (red arrow) and the $(3-4s)f_s$ (black arrow) according to equation 1. The frequency of the former one starts at 50 Hz (when s=1) and then increases up to almost 150 Hz. The latter, starts also at 50 Hz however follows a V-shape trajectory reaching 0 Hz for slip=0.75 and then increases again up to almost 150 Hz. The signatures can be easily identified due to their significant amplitudes. Such high amplitudes are the result of many factors explained in Section II in detail. At this point a simple comparison between Fig. 4 and Fig. 6 reveals the diagnostic superiority of the ZSC over the single stator current.

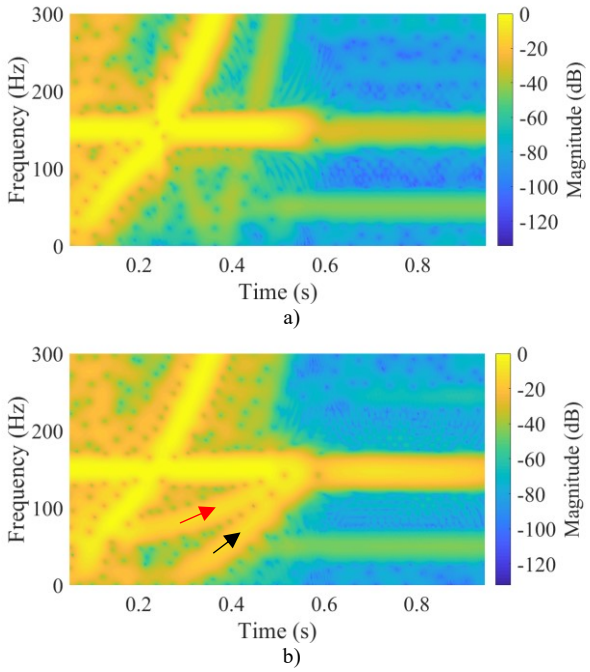

Fig. 6. STFT spectrogram of the ZSC of Motor B under: a) healthy operation and b) 1 broken bar.

IV. Experimental Testing

Motor B, which was simulated in the previous section, has been tested in the lab under heathy and faulty operation. There is only one significant difference between the simulated and the real motor; the real one has a skewed rotor by one slot pitch. It was impossible to perform the FEA simulations with a skewed rotor due to the extremely time consuming character of such simulations. Two identical induction motors have been used, one healthy and one with a broken rotor bar. The broken bar was created after drilling a hole at the connection point of a bar with the end ring as shown in Fig. 7-d.

The induction motor is coupled to BLDC generator feeding a symmetrical and variable 3-phase ohmic load as shown in Fig. 7-b. For the current measurements, three identical current sensors have been used (Fig. 7-c). The measurements were logged onto a high resolution, deep memory, 8-channel oscilloscope, which is the portable 4824 Series PicoScope. Each signal waveform was captured within 3 frames of 20 sec each, providing the ability to gather extended waveforms (60 sec) over the steady state of the motors for reliable signal representation in time and frequency domain with a sampling frequency of 10 kHz. The motor is this case starts with a soft starter. The motors were set to operate under load for an hour prior recording data, in order to reach thermal stability.

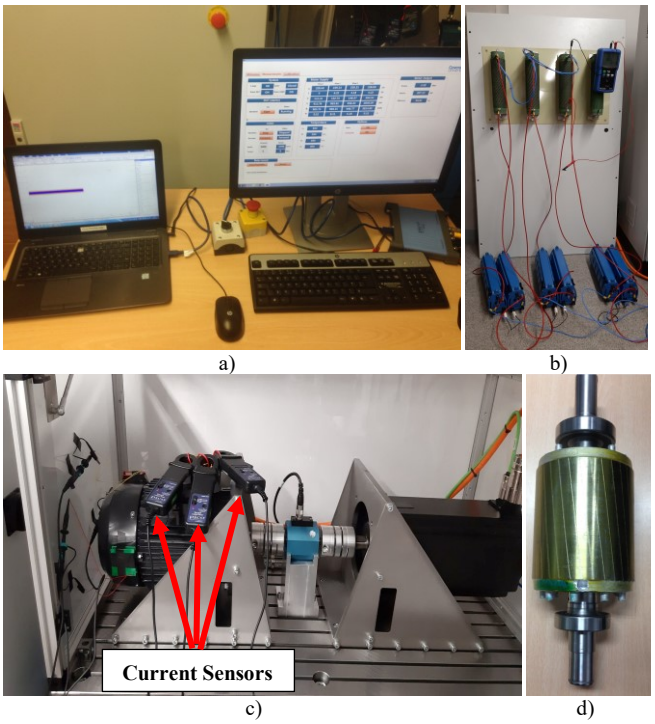

Fig. 7. Experimental set-up: a) the monitoring environment, b) the variable 3-phase ohmic load, c) the test-bench with the BLDC generator and d) rotor drilled to emulate the broken bar fault.

The extracted line and zero-sequence currents for healthy and faulty motors have been analyzed with the use of the STFT and their respective spectrograms are presented in Fig. 8 and Fig. 9.

The experimental results show that, the line current is free from noticeable broken bar fault signatures due to the limited rotor current as well as the impact of the cross currents enhanced by the skewing. The fault severity is not very high and leakage currents between the bars through the iron are responsible for masking this early fault. On the other hand, the ZSC spectrogram proves superior since the fault creates a very clear signature of frequency $(3-2s)f_s$ (red arrow) travelling from 50 Hz to 150 Hz and which is completely absent in the healthy motor. The $(3-4\,s)f_s$ (black arrow) trajectory starting from 50 Hz, dropping to 0 Hz and then increasing again to 150 Hz is also noticeable. Another interesting observation is the weakening of the PSH amplitude in the spectrogram when there is a fault. This is most possibly explained as follows: the amplitude of the PSH is normalized with respect to the ZSC fundamental, that is the third harmonic. When there is a fault, the local saturation increases and with it the third harmonic leading to lower magnitude of the PSH. Finally, a difference between experiment and simulation is the existence of the 1st and 5th line current harmonics in the ZSC spectra. Under ideal and symmetrical conditions those harmonics are absent in the ZSC however in real life machines there are inherent manufacturing and supply asymmetries leading to an amplitude difference between the three phase currents. As a result, the instantaneous sum of the three phase currents is non-zero.

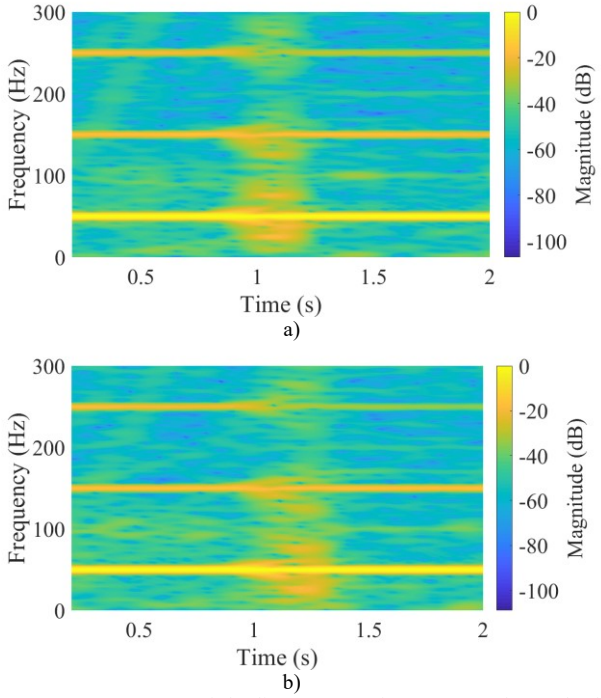

Fig. 8. STFT spectrogram of the line current of Motor B under: a) healthy operation and b) 1 broken bar (experimental testing).

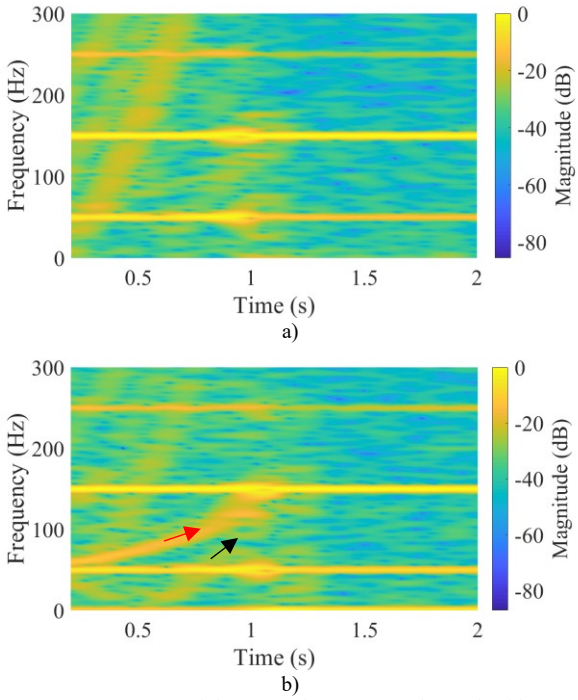

Fig. 9. STFT spectrogram of the ZSC of Motor B under: a) healthy operation and b) 1 broken bar (experimental testing).

Aiming for further generalization of the findings, a second set of experiments took place. Again, two identical induction motors (under the name Motor C) were tested. The power and general characteristics of the Motor C are similar to Motor B with the only difference lying on the number of rotor bars, which in this case is 28. Other than that, the nominal power, voltage, poles number and stator slots number is the same with Motor B. The test bench that has been prepared for the measurements is presented in Fig. 10. Two identical induction motors have been mechanically coupled in turns to a DC separately excited DC generator feeding a variable ohmic resistance and which is acting as the variable load of the system. One of the induction motors is healthy and the other has a broken rotor bar. Three current sensors have been used in order to obtain the respective current signals via a LabView DAQ. The sampling frequency has been set to 10kHz. The motors are connected to the supply via a variable 3-phase transformer, which allows for safe direct online starting.

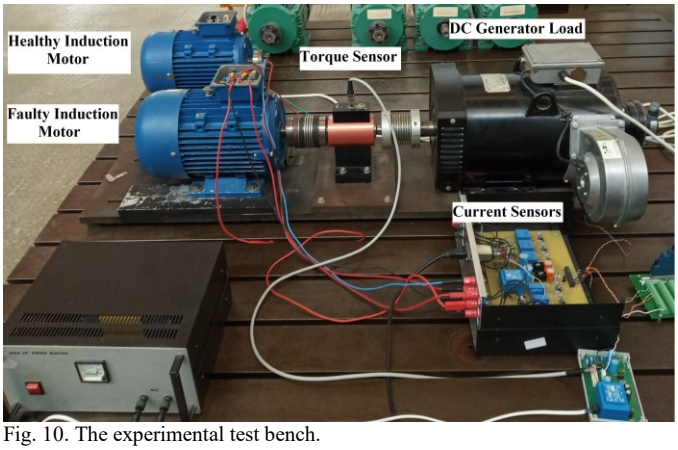

Fig. 10. The experimental test bench.

The STFT spectrograms of the line current for healthy and faulty cases of Motor C are shown in Fig. 11. It is to be noted that the main broken bar fault component $(1-2s)f_s$ is observable in both cases (black arrow), however the clarity is slightly better in the motor with the broken bar. This is due to several rotor asymmetries in the healthy motor such as the porosity of the cage and the magnetic anisotropy. Furthermore, in this particular case, the signature $(1+2s)f_s$ can be observed in the faulty motor only but with a weak amplitude (red arrow). The signatures are the ones expected by theory however there are some important aspects to be discussed here. Firstly, the $(1+2s)f_s$ signature is related to the speed ripple effect and as such is not very reliable for systems of high inertia. Secondly, the $(1-2s)f_s$ is present in the healthy motor as well, which in a real case scenario could lead to a false positive diagnostic alarm, especially when monitoring an unknown and already installed motor for the first time.

The ZSC is then calculated for both motors and afterwards their STFT spectrograms which are presented in Fig. 12. Both motors healthy and faulty have a stator asymmetry, like Motor B above, leading to the existence of the 1st and 5th stator current harmonics. However, their amplitude is weaker than the third harmonic and therefore their associated fault signatures are not observable.

The $(3-2s)f_s$ (red arrow) and $(3-4s)f_s$ (black arrow) fault related signatures are observed in both motors. That was expected since the $(1-2s)f_s$ harmonic existed in the line current of the healthy and faulty motors. Despite that, the amplitude difference is extraordinary between them. To be more specific, the third harmonic fault sidebands have similar amplitudes with the ZSC fundamental in the faulty motor (Fig. 12-b). The amplitude difference between healthy and faulty is approximately 20 dB, which makes the fault detection very reliable. It is to be noted that the amplitude of the $(3-2s)f_s$ signature is approximately -6 dB under fault. Therefore, the fault sensitivity is significantly improved via the ZSC when considering signature amplitudes of approximately -40 dB in the stator current. One interesting but expected characteristic between the two motors is the acceleration time up to the steady state. It is obvious that the faulty motor has a shorter transient and this is due to the increase in the rotor resistance when a bar breaks. This causes the shifting of the torque-speed characteristic to the left leading to higher starting torque and consequently faster acceleration to the steady state.

Additionally, one more powerful trajectory is noted in the faulty motor while absent in the healthy one and this the sf_s starting from 50 Hz and ending at 0 Hz. This signature has been associated with the detection of broken rotor bars through the stray axial flux, however it has never before associated with the ZSC.

To conclude this analysis, it is worth mentioning that no mixed eccentricity harmonics $\left[k \pm \frac{(1-s)}{p}\right] f_s, k \in \mathbb{N}$, were observed in the spectra of the line current under healthy nor faulty motor operation. Despite that, such harmonics are detectable only in the ZSC spectrogram of the faulty motor. To be specific, weak trajectories of the $\left[1 \pm \frac{(1-s)}{p}\right] f_s$ harmonics are observed close to 25 Hz and 75 Hz. The strongest ones however are the sidebands of the ZSC fundamental harmonic at $\left[3 \pm \frac{(1-s)}{p}\right] f_s$ located close to 125 Hz and 175 Hz. The existence of such harmonics is of importance because they relate the broken rotor bar fault with some rotor mixed eccentricity generated due to the spatially unbalanced mechanical forces of the cage.

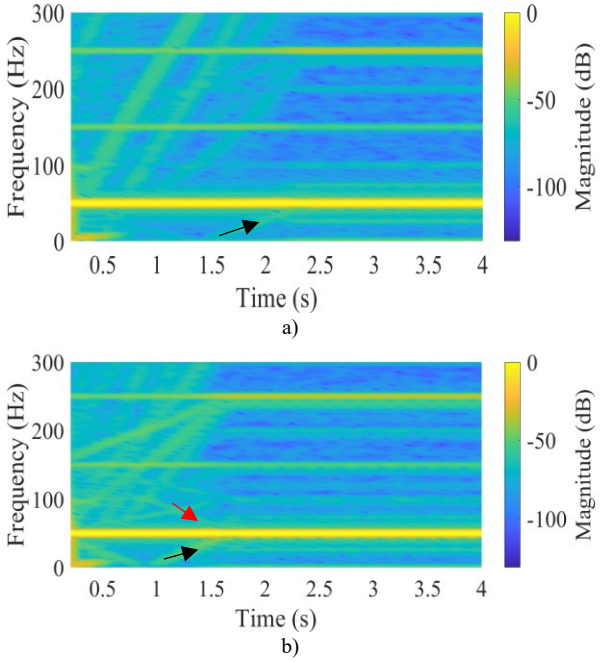

Fig. 11. STFT spectrogram of the line current of Motor C under: a) healthy operation and b) 1 broken bar (experimental testing).

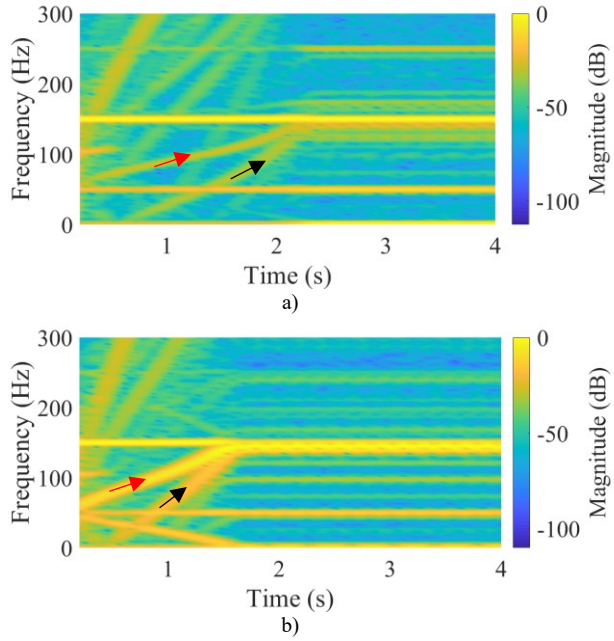

Fig. 12. STFT spectrogram of the ZSC of Motor C under: a) healthy operation and b) 1 broken bar (experimental testing).

V. Discussion and Conclusions

In this work, the zero-sequence current spectrum has been proposed for rotor electrical fault detection under transient operation (starting) of induction motors. The results demonstrate several key points of superiority versus the use of a single stator current.

Firstly, the signatures' trajectories are characterized by significantly higher amplitudes which greatly enhance the resolution of the spectrogram. A close look to Figs 3-5 shows that the main fault signature creating the V-shape has amplitude around -40 dB with respect to the fundamental. On the other hand, it is shown in Fig. 6 that the signatures of the ZSC have amplitudes around -20 dB with respect to the ZSC fundamental at 150 Hz, which is one order of magnitude greater that of the single stator current.

It was mentioned in Section II-D that the ZSC has a distinct advantage over the single stator current when very fast transients are involved. This is due to the fact that, the ZSC fundamental frequency is 3 times greater than the stator current's leading to more captured periods of the signal for a given amount of time. This is demonstrated via experimental results via Figs 8 and 9 where the ZSC is the only one of two signals to reveal trajectories of fault related signatures. This ZSC characteristic may be critical for applications utilizing motors with high starting torque, such as NEMA (National Electrical Manufacturers Association) Class D and double-cage induction motors and low inertia loads leading to fast transients.

Inherent cage asymmetries may affect the diagnosis via a single stator current. This is demonstrated in Fig. 11-a where the V-pattern is observed in a healthy motor. Moreover, when the fault occurs, the amplitude of this signature does not increase dramatically. Again the resolution is not very good. On the other hand, the ZSC fault signatures, although they also exist in the healthy motor, they increase significantly in amplitude being at similar levels with its fundamental (Fig. 12). A comparison between the two Figs 11 and 12 demonstrates the resolution superiority of the ZSC. This is due to the higher frequency that leads to higher amplitudes of the signatures due to Faraday's Law of induction together with the stronger impact of the skin effect in the rotor cage.

At a time where many cases of false positive/negative diagnostic alarms are associated with such faults, the need for improved diagnosis is tremendous from end users in industry. The paper demonstrates the improved sensitivity of the zero-sequence current, which offers significantly more information about the health status of an induction motor. The work, which relies on extensive numerical simulations via the finite element analysis and experimental testing with two different motors, builds up a solid and conclusive methodology of detecting rotor electrical faults such as broken rotor bars reliably at starting. The only limitation is that the method cannot be applied in Y connected motors with inaccessible neutral. Future work should focus on the understanding of the existence of the slip frequency in the zero-sequence current in induction motors suffering from a broken rotor bar fault, analysis under different signal processing methods such as Wavelets and image processing techniques to further investigate the spectrograms information.

References

[1] I. Boldea, "Electric generators and motors: An overview," in CES Transactions on Electrical Machines and Systems, vol. 1, no. 1, pp. 3-14, March 2017.

[2] B. Dianati, S. Kahourzade and A. Mahmoudi, "Optimization of Axial-Flux Induction Motors for the Application of Electric Vehicles Considering Driving Cycles," in IEEE Transactions on Energy Conversion, 2020 (early access).

[3] A. Oraee, R. McMahon, E. Abdi, S. Abdi and S. Ademi, "Influence of Pole-pair Combinations on the Characteristics of the Brushless Doubly Fed Induction Generator," in IEEE Transactions on Energy Conversion, 2020 (early access).

[4] K. Rana and D. C. Meena, "Self Excited Induction Generator for Isolated Pico Hydro Station in Remote Areas," 2018 2nd IEEE International Conference on Power Electronics, Intelligent Control and Energy Systems (ICPEICES), Delhi, India, pp. 821-826, 2018.

[5] J. K. H. Shek, D. G. Dorrell, M. Hsieh, D. E. Macpherson and M. A. Mueller, "Reducing bearing wear in induction generators for wave and tidal current energy devices," IET Conference on Renewable Power Generation (RPG 2011), Edinburgh, pp. 1-6, 2011.

[6] G. C. Stone, E. A. Boulter, I. Culbert, and H. Dhirani, Electrical Insulation for Rotating Machines - Design, Evaluation, Aging, Testing and Repair. IEEE Press Series on Power Engineering, 2004.

[7] L. L. Korcak and D. F. Kavanagh, "Thermal accelerated aging methods for magnet wire: A review,," International Conference on Diagnostics in Electrical Engineering (Diagnostika), pp. 1–4, 2018.

[8] F. J. T. E. Ferreira, G. Baoming and A. T. de Almeida, "Reliability and Operation of High-Efficiency Induction Motors," in IEEE Transactions on Industry Applications, vol. 52, no. 6, pp. 4628-4637, Nov.-Dec. 2016.

[9] S. Shin, J. Kim, S. B. Lee, C. Lim and E. J. Wiedenbrug, "Evaluation of the Influence of Rotor Magnetic Anisotropy on Condition Monitoring of Two-Pole Induction Motors," in IEEE Transactions on Industry Applications, vol. 51, no. 4, pp. 2896-2904, July-Aug. 2015.

[10] S. Lee, J. Hong, S. B. Lee, E. J. Wiedenbrug, M. Teska and H. Kim, "Evaluation of the Influence of Rotor Axial Air Ducts on Condition Monitoring of Induction Motors," in IEEE Transactions on Industry Applications, vol. 49, no. 5, pp. 2024-2033, Sept.-Oct. 2013.

[11] A. Bellini et al., "On-field experience with online diagnosis of large induction motors cage failures using MCSA," in IEEE Transactions on Industry Applications, vol. 38, no. 4, pp. 1045-1053, July-Aug. 2002.

[12] Yang, T.-J. Kang, S. B. Lee, J.-Y. Yoo, A. Bellini, L. Zarri and F. Filippetti, "Screening of False Induction Motor Fault Alarms Produced by Axial Air Ducts Based on the Space-Harmonic-Induced Current Components", *IEEE Trans. Indus. Elec*., Vol. 62, No. 3, pp. 1803-1813, 2015.

[13] M. Jeong, J. Yun, Y. Park, S. B. Lee and K. N. Gyftakis, "Quality Assurance Testing for Screening Defective Aluminum Die-Cast Rotors of Squirrel Cage Induction Machines," in IEEE Transactions on Industry Applications, vol. 54, no. 3, pp. 2246-2254, May-June 2018.

[14] J. Yun and S. B. Lee, "Influence of Aluminum Die-Cast Rotor Porosity on the Efficiency of Induction Machines", *IEEE Trans. Magn*., Vol. 54, No. 11, 2018.

[15] Y. Park, M. Jeong, S.B. Lee, J.A. Antonino-Daviu, M. Teska, "Influence of Blade Pass Frequency Vibrations on MCSA-based Rotor Fault Detection of Induction Motors," IEEE Transactions on Industry Applications, vol. 53, no. 3, pp. 2049-2058, May/June 2017.

[16] G. R. Bossio, C. H. De Angelo, J. M. Bossio, C. M. Pezzani and G. O. Garcia, "Separating Broken Rotor Bars and Load Oscillations on IM Fault Diagnosis Through the Instantaneous Active and Reactive Currents," in IEEE Transactions on Industrial Electronics, vol. 56, no. 11, pp. 4571-4580, Nov. 2009.

[17] J. A. Antonino-Daviu, K. N. Gyftakis, R. Garcia-Hernandez, H. Razik and A. J. M. Cardoso, "Comparative influence of adjacent and non-adjacent broken rotor bars on the induction motor diagnosis through MCSA and ZSC methods," IECON 2015 - 41st Annual Conference of the IEEE Industrial Electronics Society, Yokohama, pp. 1680-1685, 2015.

[18] Y. Park, H. Choi, S. B. Lee and K. Gyftakis, "Flux-based Detection of Non-adjacent Rotor Bar Damage in Squirrel Cage Induction Motors," 2019 IEEE Energy Conversion Congress and Exposition (ECCE), Baltimore, MD, USA, pp. 7019-7026, 2019.

[19] M. Riera-Guasp, M. F. Cabanas, J. A. Antonino-Daviu, M. Pineda-Sánchez and C. H. R. García, "Influence of Nonconsecutive Bar Breakages in Motor Current Signature Analysis for the Diagnosis of Rotor Faults in Induction Motors," in *IEEE Transactions on Energy Conversion*, vol. 25, no. 1, pp. 80-89, March 2010

[20] J. Park et al., "Evaluation of the detectability of broken rotor bars for double squirrel cage rotor induction motors," 2010 IEEE Energy Conversion Congress and Exposition, Atlanta, GA, 2010, pp. 2493-2500.

[21] J. Antonino-Daviu et al., "Detection of Broken Outer-Cage Bars for Double-Cage Induction Motors Under the Startup Transient," in IEEE Transactions on Industry Applications, vol. 48, no. 5, pp. 1539-1548, Sept.-Oct. 2012.

[22] B. Xu, L. Sun, L. Xu and G. Xu, "An ESPRIT-SAA-Based Detection Method for Broken Rotor Bar Fault in Induction Motors," in IEEE Transactions on Energy Conversion, vol. 27, no. 3, pp. 654-660, Sept. 2012.

[23] R. Puche-Panadero, M. Pineda-Sanchez, M. Riera-Guasp, J. Roger-Folch, E. Hurtado-Perez and J. Perez-Cruz, "Improved Resolution of the MCSA Method Via Hilbert Transform, Enabling the Diagnosis of Rotor Asymmetries at Very Low Slip," in IEEE Transactions on Energy Conversion, vol. 24, no. 1, pp. 52-59, March 2009.

[24] R. A. Ayon-Sicaeros, E. Cabal-Yepez, L. M. Ledesma-Carrillo and G. Hernandez-Gomez, "Broken-Rotor-Bar Detection Through STFT and Windowing Functions," 2019 IEEE Sensors Applications Symposium (SAS), Sophia Antipolis, France, pp. 1-5, 2019.

[25] V. Fernandez-Cavero, D. Morinigo-Sotelo, O. Duque-Perez and J. Pons-Llinares, "A Comparison of Techniques for Fault Detection in Inverter-Fed Induction Motors in Transient Regime," in IEEE Access, vol. 5, pp. 8048-8063, 2017.

[26] H. Douglas, P. Pillay and A. K. Ziarani, "Broken rotor bar detection in induction machines with transient operating speeds," in IEEE Transactions on Energy Conversion, vol. 20, no. 1, pp. 135-141, March 2005.

[27] G. Georgoulas et al., "The Use of a Multilabel Classification Framework for the Detection of Broken Bars and Mixed Eccentricity Faults Based on the Start-Up Transient," in IEEE Transactions on Industrial Informatics, vol. 13, no. 2, pp. 625-634, April 2017.

[28] F. Briz, M. W. Degner, P. Garcia and D. Bragado, "Broken Rotor Bar Detection in Line-Fed Induction Machines Using Complex Wavelet Analysis of Startup Transients," in IEEE Transactions on Industry Applications, vol. 44, no. 3, pp. 760-768, May-June 2008.

[29] I. P. Tsoumas, G. Georgoulas, E. D. Mitronikas and A. N. Safacas, "Asynchronous Machine Rotor Fault Diagnosis Technique Using Complex Wavelets," in IEEE Transactions on Energy Conversion, vol. 23, no. 2, pp. 444-459, June 2008.

[30] D. Morinigo-Sotelo, R. de J. Romero-Troncoso, P. A. Panagiotou, J. A. Antonino-Daviu and K. N. Gyftakis, "Reliable Detection of Rotor Bars Breakage in Induction Motors via MUSIC and ZSC," in IEEE Transactions on Industry Applications, vol. 54, no. 2, pp. 1224-1234, March-April 2018.

[31] V. Climente-Alarcon, J. A. Antonino-Daviu, A. Haavisto and A. Arkkio, "Diagnosis of Induction Motors Under Varying Speed Operation by Principal Slot Harmonic Tracking," in IEEE Transactions on Industry Applications, vol. 51, no. 5, pp. 3591-3599, Sept.-Oct. 2015.

[32] M.E.H. Benbouzid & G.B. Kliman, "What stator current processing-based technique to use for induction motor rotor faults diagnosis?", *IEEE Trans. on Energy Conv.*, Vol. 18, No. 2, pp.238-244, June 2003.

[33] K. N. Gyftakis and J. C. Kappatou, "The Zero-Sequence Current as a Generalized Diagnostic Mean in Δ-Connected Three-Phase Induction Motors," in IEEE Transactions on Energy Conversion, vol. 29, no. 1, pp. 138-148, March 2014.

BIOGRAPHIES

Konstantinos N. Gyftakis (M'11, SM'20) was born in Patras, Greece, in May 1984. He received the Diploma in Electrical and Computer Engineering from the University of Patras, Patras, Greece in 2010. He pursued a Ph.D in the same institution in the area of electrical machines condition monitoring and fault diagnosis (2010-2014). Furthermore, he worked as a Post-Doctoral Research Assistant in the Dept. of Engineering Science, University of Oxford, UK (2014-2015). Then he worked as Lecturer (2015-2018) and Senior Lecturer (2018-2019) in the School of Computing, Electronics and Mathematics and as an Associate with the Research Institute for Future Transport and Cities, Coventry University, UK.

Since 2019, he has been a Lecturer in Electrical Machines and a Member of the Institute for Energy Systems, University of Edinburgh, UK.

His research interests focus in the fault diagnosis, condition monitoring and degradation of electrical machines. He has authored/co-authored more than 100 papers in international scientific journals and conferences and a chapter for the book: "Diagnosis and Fault Tolerance of Electrical Machines, Power Electronics and Drives", IET, 2018. He is an IEEE Senior Member, as well as member of the IEEE IAS and IEEE IES.

Dionysios V. Spyropoulos (S'07, M'11) was born in Patras, Greece, in September 1985. He received his Diploma degree in Electrical and Computer Engineering in 2009 from the University of Patras, where he is currently working towards the Ph.D. degree in electric drive systems at the Electromechanical Energy Conversion Laboratory. His current research interests include electric drive systems, power electronics, motor fault diagnosis, electric machines and drives monitoring. Mr. Spyropoulos is a Member of the IEEE and a Member of the Technical Chamber of Greece.

Epaminondas D. Mitronikas (M'07) was born in Agrinio, Greece, in March 1973. He received the Dipl.-Eng. degree in electrical and computer engineering and the Ph.D. degree from the Department of Electrical and Computer Engineering, University of Patras, Rio-Patras, Greece, in 1995 and 2002, respectively. He is an Assistant Professor at the Department of Electrical and Computer Engineering, University of Patras. His research interests include power electronics, electrical machines, modeling, design, digital control and diagnostics of electric motor drive systems, and control of low power electromechanical systems. Dr. Mitronikas is a member of IEEE and the Technical Chamber of Greece.